CHAPTER III
PROGNOSTIC SIGNIFICANCE OF PEROXIREDOXIN 1 AND EZRIN-RADIXIN-MOESIN-BINDING PHOSPHOPROTEIN 50 IN CHOLANGIOCARCINOMA

3.1 Introduction

Cholangiocarcinoma (CCA) is a primary liver cancer occurring in the bile duct epithelium. Although a rare tumor worldwide, CCA has a high incidence in Southeast Asia, especially in northeastern Thailand, where infection with the liver fluke, *Opisthorchis viverrini*, is endemic (Bower et al., 1998; Sripa et al., 2007). *O. viverrini* infection is transmitted by the consumption of raw or undercooked freshwater fish in regional dishes which contain the metacercarial (i.e, infective) stage of the fluke. Once consumed, the immature flukes migrate up the ampulla of Vater to the biliary tree and mature in the small intrahepatic bile ducts (Sripa et al., 2008). An estimated 6 million people are infected with *O. viverrini* in Thailand (Sripa et al., 2003), where it has long been hypothesized that chronic infection with *O. viverrini* is associated with the development of CCA (Sriamporn et al., 2004; Sriamporn et al., 2005; Sripa et al., 2007). Indeed, there may be no stronger link between an eukaryotic organism and a malignant neoplasm than that between *O. viverrini* and CCA, which led the World Health Organization's International Agency for Research on Cancer to classify *O. viverrini* as a Group 1 carcinogen (Bouvard et al., 2009).

Advanced CCA has an extremely poor prognosis. Over the past 30 years, much effort has been devoted to improving the survival rate of CCA patients. Currently, the complete surgical resection of all detectable tumors from the liver and bile duct has been shown to improve the five-year survival rate, but surgical resection must be done before advanced stages of CCA. Unfortunately, the majority of patients present with an advanced stage of CCA, which is not amenable to this surgical intervention. Hence, the discovery of novel biomarkers to further refine prognosis and response to treatment is of great important.

Two-dimensional gel electrophoresis (2-DE) and mass spectrometry (MS) are still the method of choice for the analysis of proteins above approximately 20-30 kDa. As the technique itself is difficult to reproduce and is therefore not applicable as a diagnostic tool, it can however be used to discovery of tumor markers, as has been shown by several groups (Lomnytska et al., 2010; Bai et al., 2011; Jeong et al., 2011)

Recently, a comparative proteomic study of membrane proteins from four human *O. viverrini* associated CCA cell lines with non-tumor H69 biliary cell line as a control identified annexin A2 (ANXA2) as a prognostic marker for predicting the outcome of CCA patients (Yonglitthipagon et al., 2010). In the present study, we not only attempt to characterize cytosolic protein profiles from CCA cell lines with different tumor forming capabilities and non-tumor H69 biliary cell line, but also the prognostic significance of candidate proteins in the human liver, under normal condition and in CCA.

3.2 Materials and Methods

3.2.1 Cell lines and cell culture

Four human CCA cell lines, M156, K100, M139 and M213, were isolated from CCA patients from north eastern Thailand as described elsewhere (Sripa et al., 2005). In all cases, CCA was associated with chronic *O.viverrini* infection. Approval for use of the tissue was obtained from the Human Research Ethics Committee of Khon Kaen University, Thailand. CCA tissues were histologically diagnosed as follows: moderately differentiated adenocarcinoma (M156), poorly differentiated adenocarcinoma (K100), squamous cell carcinoma (M139), and adenosquamous cell carcinoma (M213). H69 cells, an 'immortalized' non-malignant human cholangiocyte cell line, and the CCA cell lines were cultured as previously described (Yonglitthipagon et al., 2010).

3.2.2 Tissue samples

In this study, CCA tissues were obtained after informed consent from the patients who underwent hepatectomy at Srinagarind hospital, Khon Kaen University, Thailand as described elsewhere (Yonglitthipagon et al., 2010). Of the 301 liver fluke-associated CCA samples analyzed, 203 were from males and 98 were from females at a ratio of 2:1. The mean (±SD) age in years was 55 ± 9.4 years

(range, 31-75 years). Most of the patients were at an advanced CCA stage, 73.9% (n = 210) with lymphatic invasion, 53.1% (n = 152) with vascular invasion, and 39.6% (n = 112) with perineural invasion. The histopathologic grade of differentiation of the tumors was assessed to be well-differentiated histophotological type in 53 (35%) patients. The majority of patients (63.5%) possessed a tumor size > 5 cm.

3.2.3 Extraction of cytosolic proteins

The cell lines were examined under a phase-contrast microscope to ensure that they were over 70% confluence before lysis. The culture medium was discarded and the cells washed with 0.25 M sucrose three times on ice. Cells were scraped thoroughly with a scraper in 0.25 M sucrose containing 1% Protease Inhibitor Mix (GE healthcare). The cells were collected and centrifuged at 1,500 ×g for 5 min at 4°C. The pellets were resuspended in lysis buffer containing 7 M urea, 2 M thiourea, 4% CHAPS, 2% IPG buffer pH 3-10 nonlinear (GE healthcare), 40 mM DTT, and 1% Protease Inhibitor Mix and allowed to lyse on ice for 15 min. Cell lysates were sonicated according to the manufacturer's instructions (Sonics & Materials Inc. VCX 400, USA) and incubated for 2 h at 4°C. The lysate was then centrifuged at 600 ×g for 10 min to remove the nuclei and unlysed cells. The supernatant containing cytosolic protein was transferred to a clean tube and centrifuged at 10,000 ×g for 15 min to remove the mitochondrial fraction. The supernatant was collected again and centrifuged at 100,000 ×g for 2 h to generate a pellet containing the enriched microsomal fraction and the supernatant representing the cytosolic fraction. The total protein concentration in the cytosolic fraction was determined by Bradford Assay using a VersaMax™ absorbance microplate reader with SOFTMax pro (Molecular Devices Corporation California, USA) at 595 nm. Cytosolic proteins of each cell line were then ready for 2-DE.

3.2.4 Two-dimensional gel electrophoresis and image analysis

Total protein (100 μg) from CCA cell lines and H69 as a control were separated by 2-DE. Isoelectric focusing was performed using IPG strips (pH 3-10NL, 7 cm) on an IPGphor isoelectric focusing cell (GE Healthcare) and second-dimension SDS-PAGE using a Hoefer system (GE Healthcare) as described previously (Yonglitthipagon et al., 2010). After electrophoresis, the protein spots were visualized by CBR-250 (GE healthcare) staining. Stained gels were scanned using an

ImageScanner (GE healthcare) and the 2-DE images of each cell line were compared using ImageMaster™ 2D Platinum 6.0 software (GE healthcare).

3.2.5 In-gel digestion of 2-DE, MALDI-TOF MS analysis and database search

Protein spots that were unique to or stained more intensely in CCA cell lines compared with H69 cells were excised from the gel and transferred to V-bottom 96-well microtitre plates. Tryptic digestions were performed on an EttanTM Spot Handling Workstation robot (Amersham Biosciences) according to the manufacturer's specifications. The 10 mg of matrix solution, α-cyano-4-hydroxycinnamic acid (Bruker Daltonik GmbH, Germany), was prepared by dissolving to saturation in 50% acetronitrile/water with 0.1% trifluoroacetic acid and then mixed with equal volumes of tryptic peptides with matrix solution. The mixture (1 μL) was spotted onto a steel target surface (MTP 384 ground steel, Bruker Daltonik) and dried at room temperature. Mass spectra were recorded on an Autoflex MALDI-TOF-mass spectrometer (Bruker Daltonik) at a maximum accelerating potential of 19 kV and in reflector mode. The *m/z* range was from 400 to 4000. The MALDI-TOF-MS was calibrated using trypsin auto-digestion peptide signals and matrix ion signals. Typically, 100 shots were accumulated from three to five different positions within a sample spot. The mass spectra were analyzed using MALDI evaluation software (Amersham Biosciences; release version 2.0). Proteins were identified by peptide mass fingerprinting using Mascot (http://www.matrixscience.com) in searches against the NCBInr (NCBInr 2009.04.03). The parameters used in the Mascot searches were as follows: (1) taxonomy was restricted to *Homo sapiens*, (2) trypsin specified with the allowance for one missed cleavage, (3) peptide mass tolerance fragment mass tolerance were set to 100 ppm and ± 0.5 Da, respectively and (4) carbamidomethyl and oxidized methionine were chosen as the fixed and variable modifications, respectively. Protein hits were considered significant if the Mascot score was greater than 43 (significance level, $p < 0.05$). Other criteria for confident identification were that the protein match should have at least 17% sequence coverage and match at least 11 peptides. If peptides matched to multiple members of a protein family, proteins with shared peptides were grouped and the highest scoring protein was selected as the representative protein.

3.2.6 Tissue microarray and immunohistochemistry

Tissue microarrays (TMAs) containing 301 human CCA patient tissues were constructed by the Department of Pathology, Faculty of Medicine, Khon Kaen University, Thailand (Fedor et al., 2005). Prior to TMA construction, all tissue slides were histopathologically re-evaluated by experienced histopathologist (Chawalit Pairojkul). The extent of invasion by the cancer was determined in both the interface of the growing tumor border and the adjacent liver tissue. Pathologic vascular invasion was defined as the presence of a tumor cell emboli within a vessel space, which were identified by associated fibrin clot and/or an endothelial cell lining. Lymphatic invasion was defined as being present when cancer cells were detected floating within an endothelium-lined space. Perineural invasion was defined as tumor invading the perineural sheath or endoneurium.

Immunohistochemical (IHC) reactions were performed on 4 μm-thick sections of TMA silane-coated slides (Sigma, St. Louis, MO, USA) by an immunoperoxidase method as described (Yonglitthipagon et al., 2010). The TMA sections probed with rabbit polyclonal anti-Peroxiredoxin 1 (Abcam Inc., USA) diluted 1:500 (v/v) or rabbit polyclonal anti-EBP50 (Abcam) diluted 1:400 (v/v) in PBS and incubated overnight at 4 °C. After rinsing for 3 × 5 min with PBS the sections were incubated with biotin-conjugated goat anti-rabbit immunoglobulin (Zymed Labs., San Francisco, CA) diluted 1:300 (v/v) in PBS and incubated at RT for 1 h. The sections were then incubated with a horse radish peroxidase-conjugated streptavidin (Zymed Labs.) diluted 1:300 (v/v) in PBS at RT for 1 h. Sections were rinsed with PBS for 2 × 10 min, after which the sections were developed with DAB (Sigma Chemical Co.). The sections were counterstained with Mayer's haematoxylin, dehydrated, cleared in xylene and mounted in Permount®.

3.2.7 Immunohistochemical and statistical analysis

Immunoreactivity was evaluated independently by three researchers (PY, BS and CP) who were blinded to patient status and outcome. The percentage of positive tumor cells was determined using interactive stereological immunoscoring based on systematic random sampling (van Diest et al., 1997), and the mean score was calculated. In this study, the percentage of positive cells expressing PRX1 and

EBP50 were categorized as follows: <10% (-), ≥10% (+) as described elsewhere (Zhuang et al., 2008).

Statistical analyses of the data were performed with SPSS version 16.0 statistical package as described elsewhere (Yonglitthipagon et al., 2010). For cross-sectional analyses, the chi-square test was utilized to analyze the relationship between PRX1 and EBP50 expressions and categorical variables regarding clinical pathology parameters (e.g., age group, gender and histotype). The Kaplan–Meier method was used to calculate cumulative survival. Differences in survival between low expression and high expression groups were analyzed for significance by the log-rank method. The Cox-regression model was used to perform multivariate analysis, and values of $p < 0.05$ were considered statistically significant.

3.3 Results

3.3.1 2-DE profiling of differentially expressed proteins between H69 and CCA cells

In order to examine the differential protein expression profiles of CCA cell lines, three biological replicates for each cell type (M156, KKU100, M139, M213 and H69) were generated. The separated protein spots were visualized on 2D gels by CBR-250 staining, and displayed good reproducibility for protein spot quantification and comparative analysis. Figure 3.1 shows representative 2-DE maps of each CCA cell lines (M156, K100, M139 and M213, respectively) with spots subjected to MALDI-TOF MS and their identification numbers; the identified spots are listed in Table 3.1. The experimental p*I* and *Mr* values of identified proteins correlated with the theoretical values reported in the NCBInr database. As reported previously (Pucci-Minafra et al., 2002; Fontana et al., 2004; Pucci-Minafra et al., 2006), some observed differences between the experimental and theoretical p*I*/*Mr* values and the presence of different isoforms of the same protein (data not shown) could reflect post-translational modifications or splice variants.

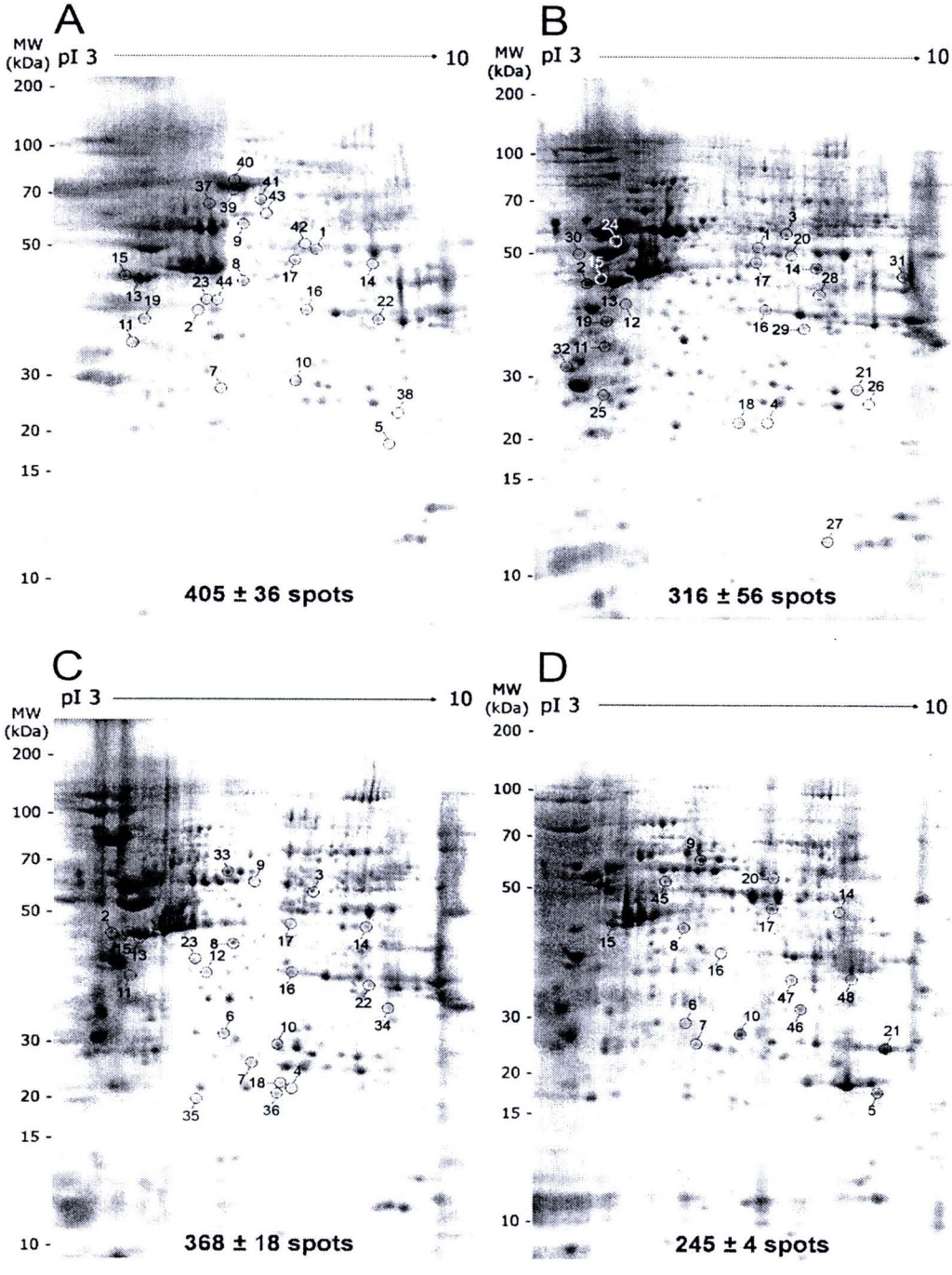

Figure 3.1 2-DE maps of cytosolic proteins of 4 human cholangiocarcinoma cell lines; M156, moderately differentiated adenocarcinoma (A), KKU-100, poorly differentiated adenocarcinoma (B), M139, squamous cell carcinoma (C) and M213, adenosquamous cell carcinoma (D). Number of spots on 2-DE showed a total of 405±36, 316±56, 368±18 and 245±34 (mean±S.E. of three biological replicates) for the M156, KKU-100, M139 and M213, respectively.

Table 3.1 List of differentially expressed cytosolic proteins from 4 CCA cell lines identified by MALDI-TOF MS

No.[a]	A/N[b]	Description	Biological process	MS[c]	MP /TP[d]	CO[e]	*Mr*	p*I*	H69	M156	K100	M139	M213
1	gi|34147630	Tu translation elongation factor	Signal transduction	194	28 / 38	65	50.19	7.26	-	+	+	-	-
2	gi|1710248	Protein disulfide isomerase	Protein metabolic process	69	7 / 36	17	46.51	4.95	-	-	+	+	-
3	gi|169404695	Chain A, Pyruvate Kinase M2	Carbohydrate metabolic process	185	22 / 51	38	57.09	8	-	-	+	+	-
4	gi|544759	Biliverdin-IX beta reductase isozyme I	Unknown	110	10 / 27	51	21.96	7.31	-	-	+	+	-
5	gi|5031635	Cofilin 1	Cellular component morphogenesis	202	18 / 55	75	18.72	8.22	-	+	-	-	+
6	gi|4505773	Prohibitin	Nucleic and nucleotide metabolic process	211	17 / 42	73	29.84	5.57	-	+	-	+	+
7	gi|4758638	Peroxiredoxin 6	Oxygen and reactive oxygen species metabolic process	147	17 / 50	79	25.13	6	-	+	-	+	+
8	gi|119581639	Proteasome	Protein metabolic process	240	28 / 53	65	43.22	5.97	-	+	-	+	+
9	gi|4502643	Chaperonin containing TCP1	Protein metabolic process	306	38 / 80	65	58.44	6.23	-	+	-	+	+
10	gi|999892	Triosephosphate Isomerase	Carbohydrate metabolic process	220	19 / 42	84	26.81	6.51	-	+	-	+	+
11	gi|18314408	Nucleophosmin	Nucleic and nucleotide metabolic process	78	11 / 50	27	32.73	4.59	-	+	+	+	-
12	gi|15277503	ACTB protein	Cellular component morphogenesis	164	21 / 44	67	40.54	5.35	-	+	+	+	-
13	gi|62897681	Calreticulin	Protein metabolic process	222	20 / 38	58	47.06	4.3	-	+	+	+	-
14	gi|48145549	PGK1	Carbohydrate metabolic process	354	36 / 46	62	44.97	8.3	-	+	+	+	+
15	gi|90111766	Keratin 19	Cellular component organization	375	34 / 49	75	44.08	5.04	-	+	+	+	+

Table 3.1 List of differentially expressed cytosolic proteins from 4 CCA cell lines identified by MALDI-TOF MS (Cont.)

No.[a]	A/N[b]	Description	Biological process	MS[c]	MP /TP[d]	CO[e]	*Mr*	p*I*	H69	M156	K100	M139	M213
16	gi|119582950	Annexin A1	Intracellular protein transport	252	28 / 45	77	40.48	6.57	-	+	+	+	+
17	gi|203282367	Enolase 1	Carbohydrate metabolic process	174	21 / 44	53	47.35	6.99	-	+	+	+	+
18	gi|3023905	Glutathione S-transferase	Immune system process	148	12 / 34	57	23.64	6.89	-	-	+	+	-
19	gi|4502107	Annexin 5	Signal transduction	176	17 / 27	54	35.97	4.94	-	+	+	-	-
20	gi|197210452	Uridine monophosphate synthetase	Unknown	95	11 / 53	16	52.71	6.81	-	-	+	-	+
21	gi|4503727	FK506 binding protein 3, 25kDa	Negative regulation of apoptosis	109	12 / 38	44	25.22	9.26	-	-	+	-	+
22	gi|67464043	Human Liver Gapdh	Carbohydrate metabolic process	185	19 / 29	57	36.48	8.53	-	+	-	+	-
23	gi|82195535	Gamma-actin	Cellular component morphogenesis	165	22 / 50	64	42.09	5.3	-	+	-	+	-
24	gi|119602173	Heat shock protein 90kDa	Response to stress	117	16 / 35	27	57.87	4.92	-	-	+	-	-
25	gi|4507651	Tropomyosin 4 isoform 2	Cellular component organization	146	14 / 31	43	28.62	4.67	-	-	+	-	-
26	gi|21620034	ZSCAN21 protein	Nucleic and nucleotide metabolic process	43	12 / 20	24	26.69	9.45	-	-	+	-	-
27	gi|46409504	Hypothetical protein LOC400165	Unknown	46	42 / 82	38	13.69	8.66	-	-	+	-	-
28	gi|123266507	guanylatecyclase 1, soluble, beta 2	Nucleic and nucleotide metabolic process	44	39 /56	19	44.95	8.84	-	-	+	-	-
29	gi|7669492	Glyceraldehyde-3-phosphate dehydrogenase	Carbohydrate metabolic process	67	42 / 55	18	36.21	8.57	-	-	+	-	-

Table 3.1 List of differentially expressed cytosolic proteins from 4 CCA cell lines identified by MALDI-TOF MS (Cont.)

No.[a]	A/N[b]	Description	Biological process	MS[c]	MP /TP[d]	CO[e]	*Mr*	p*I*	H69	M156	K100	M139	M213
30	gi|5174735	Tubulin, beta, 2	Intracellular protein transport	148	23 / 36	57	50.26	4.79	-	-	+	-	-
31	gi|7108915	Glucocorticoid receptor AF-1	Signal transduction	69	42 / 85	19	46.58	9.08	-	-	+	-	-
32	gi|49119653	YWHAZ protein	Signal transduction	153	16 / 37	45	30.11	4.72	-	-	+	-	-
33	gi|189502784	Heat shock protein 60kD	Response to stress	249	30 / 48	59	60.81	5.83	-	-	-	+	-
34	gi|4504447	hnRNP A2/B1	Intracellular protein transport	89	19 / 46	44	36.04	8.67	-	-	-	+	-
35	gi|4507669	Tumor protein, translationally-controlled 1	Immune system process	116	16 / 41	61	19.69	4.84	-	-	-	+	-
36	gi|55960374	Transgelin 2	Muscle contraction	88	10 / 31	45	21.24	7.63	-	-	-	+	-
37	gi|31542947	Chaperonin	Protein metabolic process	230	26 / 50	52	61.19	5.7	-	+	-	-	-
38	gi|4505591	Peroxiredoxin 1	Oxygen and reactive oxygen species metabolic process	243	19 / 33	76	22.32	8.27	-	+	-	-	-
39	gi|46249758	Ezrin	Intracellular protein transport	258	28 / 31	43	69.31	5.94	-	+	-	-	-
40	gi|4505257	Moesin	Intracellular protein transport	146	26 / 46	33	67.89	6.08	-	+	-	-	-
41	gi|5803181	Hsp70/Hsp90	Response to stress	129	38 / 85	55	63.23	6.4	-	+	-	-	-
42	gi|52632385	hnRNP L	Nucleic and nucleotide metabolic process	104	13 / 28	35	51.16	7.22	-	+	-	-	-
43	gi|38013966	TKT protein	Lipid metabolic process	303	22 / 26	46	58.74	6.51	-	+	-	-	-
44	gi|167860126	Serine proteinase inhibitor	Protein metabolic process	278	25 / 42	73	42.53	5.72	-	+	-	-	-
45	gi|12803727	Keratin 7	Cellular component organization	210	22 / 33	46	51.44	5.42	-	-	-	-	+

Table 3.1 List of differentially expressed cytosolic proteins from 4 CCA cell lines identified by MALDI-TOF MS (Cont.)

No.[a]	A/N[b]	Description	Biological process	MS[c]	MP /TP[d]	CO[e]	*Mr*	p*I*	H69	M156	K100	M139	M213
46	gi|42476281	Voltage-dependent anion channel 2	Ion transport	147	13 / 25	54	32.06	7.49	-	-	-	-	+
47	gi|5174447	Guanine nucleotide binding protein	Intracellular protein transport	225	21 / 32	56	35.51	7.61	-	-	-	-	+
48	gi|54303910	Aging-associated gene 9 protein	Carbohydrate metabolic process	155	14 / 27	43	36.19	8.57	-	-	-	-	+

Note: [a]Numbers correspond to Figure 3.1. [b]NCBInr database accession numbers. [c]Mascot score (MS= -10*Log (P); where *P* is the pobability that the observed match is a random even from MS analysis. [d]The number of matched peaks/total peaks in MS analysis. [e]Percentage of sequence coverage. The presence of a protein in the relevant study is denoted with a '+' and the absence with a '-'.

3.3.2 Protein identification by MALDI-TOF MS

Using 2D gel replicates, the identical and differential protein expression in 4 CCA cell lines subtracted from H69 were measured. In Table 3.1, the proteins, corresponding to 48 spots, which were expressed only in CCA cell lines but not in H69 are shown, together with the MS identification parameters. To classify the biological significance of the differentially expressed proteins, MS-identified proteins were classified into molecular and biological functional groups using the PANTHER database. Several of the identified proteins have been associated with cancer in previous studies (David et al.; Chang et al., 2003; Zhong et al., 2003; Desmetz et al., 2008), such as HSP60 and HSP70/HSP90, enolase-alpha and hnRNPs. As shown in Figure 3.2, MALDI-TOF MS analysis and peptide mass finger printing of the tryptic digests subsequently identified protein spot 38 as PRX1 (Figure 3.2A), spot 39 as ezrin (Figure 3.2B) and spot 40 as moesin (Figure 3.2C). Peroxiredoxin 1 (PRX1) and ezrin-radixin-moesin-binding phosphoprotein 50 (EBP50); a binding partner of ezrin and moesin, were selected for further verification, as their expression levels correlate with tumor progression in other cancers (Kim et al., 2007; Song et al., 2007; Georgescu et al., 2008; Chhipa et al., 2009) but their prognostic utilities in human *O. viverrini*-associated CCA has not been explored.

A

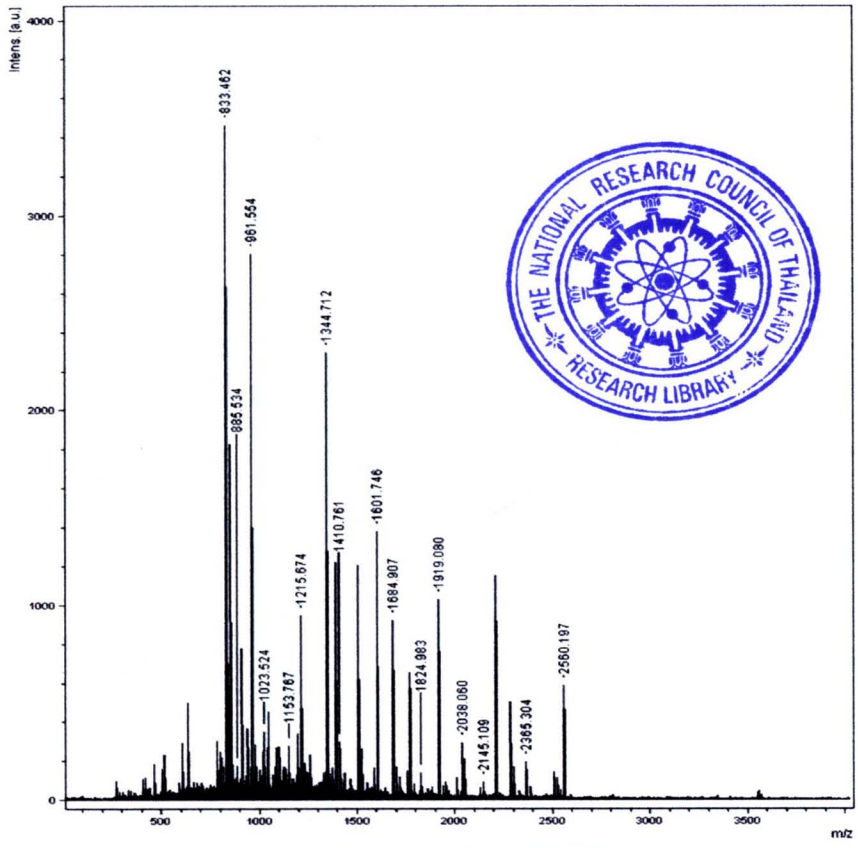

1 MSSGNAKIGH PAPNFKATAV MPDGQFKDIS LSDYKGKYVV FFFYPLDFTF
51 VCPTEIIAFS DRAEEFKKLN CQVIGASVDS HFCHLAWVNT PKKQGGLGPM
101 NIPLVSDPKR TIAQDYGVLK ADEGISFRGL FIIDDKGILR QITVNDLPVG
151 RSVDETLRLV QAFQFTDKHG EVCPAGWKPG SDTIKPDVQK SKEYFSKQK

Figure 3.2 Peptide mass fingerprint (PMF) of tryptic digests of peroxiredoxin 1(A), ezrin (B) and moesin (C) obtained by MALDI-TOF MS. The spectrum displays *m/z* ratio (*x-axis*) and relative intensity (*y-axis*) of the peptides identified. Matched peptides of peroxiredoxin 1, ezrin and moesin were 76%, 43% and 33% protein sequence coverage showed by red and underline, respectively. Protein identification using PMF data was performed with the Mascot search engine; acquired spectra were processed and search against the NCBInr database.

B

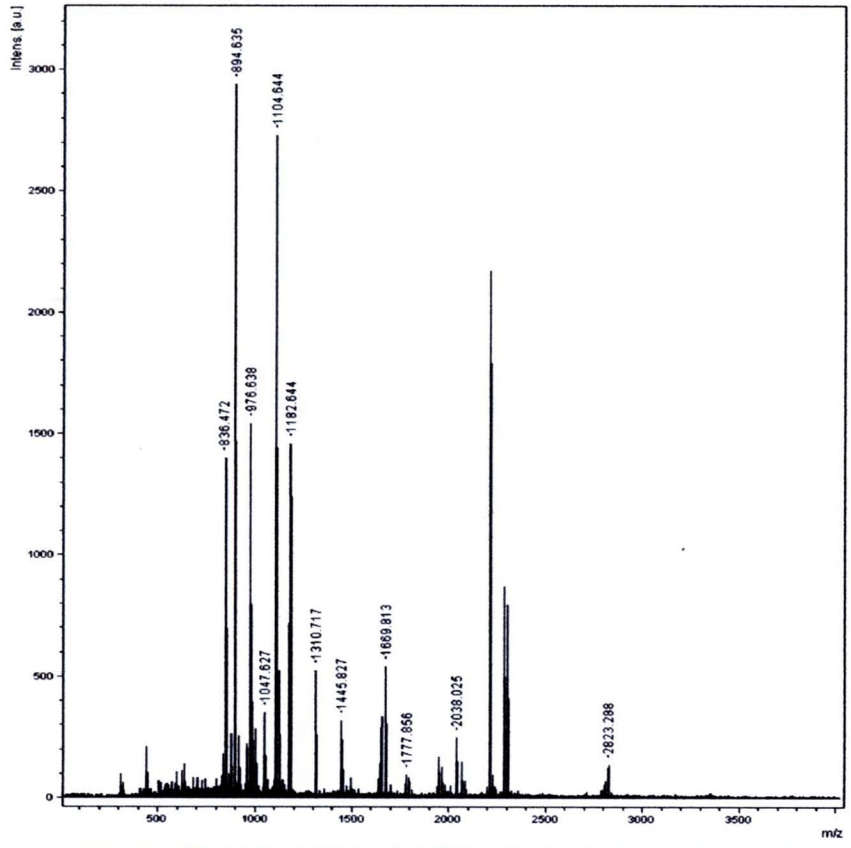


```
  1 MPKPINVRVT TMDAELEFAI QPNTTGKQLF DQVVKTIGLR EVWYFGLHYV
 51 DNKGFPTWLK LDKKVSAQEV RKENPLQFKF RAKFYPEDVA EELIQDITQK
101 LFFLQVKEGI LSDEIYCPPE TAVLLGSYAV QAKFGDYNKE VHKSGYLSSE
151 RLIPQRVMDQ HKLTRDQWED RIQVWHAEHR GMLKDNAMLE YLKIAQDLEM
201 YGINYFEIKN KKGTDLWLGV DALGLNIYEK DDKLTPKIGF PWSEIRNISF
251 NDKKFVIKPI DKKAPDFVFY APRLRINKRI LQLCMGNHEL YMRRRKPDTI
301 EVQQMKAQAR EEKHQKQLER QQLETEKKRR ETVEREKEQM MREKEELMLR
351 LQDYEEKTKK AERELSEQIQ RALQLEEERK RAQEEAERLE ADRMAALRAK
401 EELERQAVDQ IKSQEQLAAE LAEYTAKIAL LEEARRRKED EVEEWQHRAK
451 EAQDDLVKTK EELHLVMTAP PPPPPPVYEP VSYHVQESLQ DEGAEPTGYS
501 AGLSSEGIRD DGNEEKRITE AEKNERVQRQ LLTLSSELSQ ARDENKRTHN
551 DIIHNENMRQ GRDKYKTLRQ IRQGNTKQRI DEFEAL
```

Figure 3.2 Peptide mass fingerprint (PMF) of tryptic digests of peroxiredoxin 1(A), ezrin (B) and moesin (C) obtained by MALDI-TOF MS. The spectrum displays *m/z* ratio (*x-axis*) and relative intensity (*y-axis*) of the peptides identified. Matched peptides of peroxiredoxin 1, ezrin and moesin were 76%, 43% and 33% protein sequence coverage showed by red and underline, respectively. Protein identification using PMF data was performed with the Mascot search engine; acquired spectra were processed and search against the NCBInr database (Cont.).

C

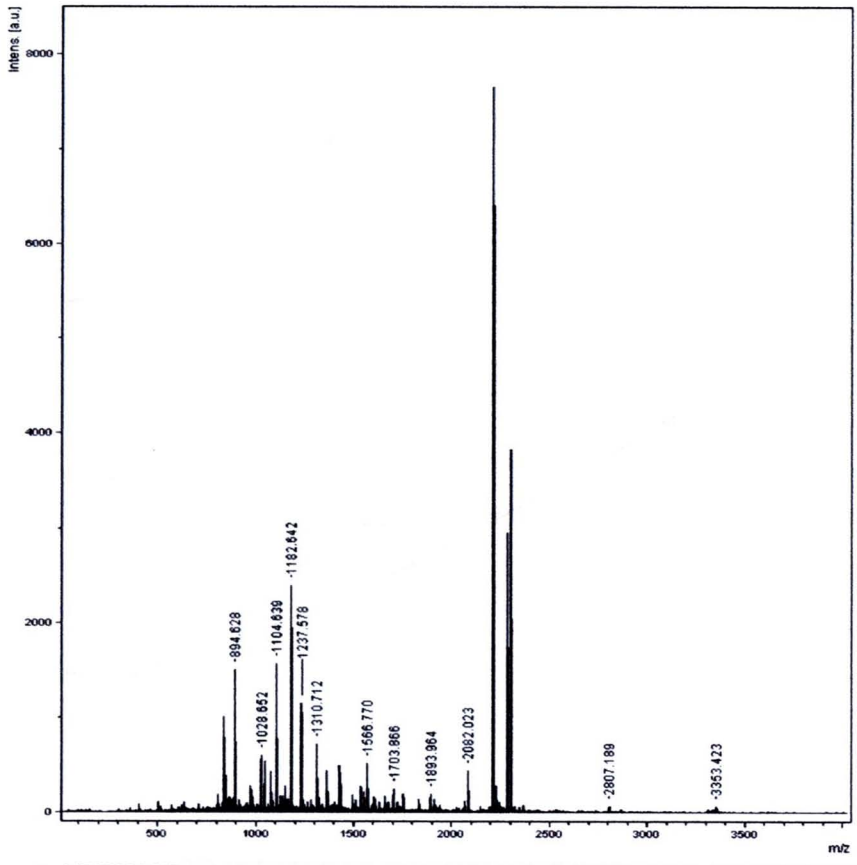


```
  1 MPKTISVRVT TMDAELEFAI QPNTTGKQLF DQVVKTIGLR EVWFFGLQYQ
 51 DTKGFSTWLK LNKKVTAQDV RKESPLLFKF RAKFYPEDVS EELIQDITQR
101 LFFLQVKEGI LNDDIYCPPE TAVLLASYAV QSKYGDFNKE VHKSGYLAGD
151 KLLPQRVLEQ HKLNKDQWEE RIQVWHEEHR GMLREDAVLE YLKIAQDLEM
201 YGVNYFSIKN KKGSELWLGV DALGLNIYEQ NDRLTPKIGF PWSEIRNISF
251 NDKKFVIKPI DKKAPDFVFY APRLRINKRI LALCMGNHEL YMRRRKPDTI
301 EVQQMKAQAR EEKHQKQMER AMLENEKKKR EMAEKEKEKI EREKEELMER
351 LKQIEEQTKK AQQELEEQTR RALELEQERK RAQSEAEKLA KERQEAEEAK
401 EALLQASRDQ KKTQEQLALE MAELTARISQ LEMARQKKES EAVEWQQKAQ
451 MVQEDLEKTR AELKTAMSTP HVAEPAENEQ DEQDENGAEA SADLRADAMA
501 KDRSEEERTT EAEKNERVQK HLKALTSELA NARDESKKTA NDMIHAENMR
551 LGRDKYKTLR QIRQGNTKQR IDEFESM
```

Figure 3.2 Peptide mass fingerprint (PMF) of tryptic digests of peroxiredoxin 1(A), ezrin (B) and moesin (C) obtained by MALDI-TOF MS. The spectrum displays *m/z* ratio (*x-axis*) and relative intensity (*y-axis*) of the peptides identified. Matched peptides of peroxiredoxin 1, ezrin and moesin were 76%, 43% and 33% protein sequence coverage showed by red and underline, respectively. Protein identification using PMF data was performed with the Mascot search engine; acquired spectra were processed and search against the NCBInr database (Cont.).

3.3.3 Immunohistochemistry of PRX1 and EBP50

IHC analysis was carried out on the TMA (n = 301) using anti-PRX1 and anti-EBP50 rabbit polyclonal antibodies to confirm PRX1 and EBP50 expression changes during cholangiocarcinogenesis. Weak staining of PRX1 (Figure 3.3A) and EBP50 (Figure 3.3C) were observed in the cytoplasm and on the apical surface of normal hepatocytes and cholangiocytes. In contrast, PRX1 (Figure 3.3B) and EBP50 (Figure 3.3D) were highly expressed in the majority of the corresponding CCA tissues, concentrated in the cytoplasm and moderate labeling on the on the apical surface. Positive expression of EBP50 and PRX1 was found in the biopsies from 180 patients (59.8%) and 103 patients (34.3%), respectively. Statistical analysis showed that over-expression of PRX1 was found to be associated with an age-related effect in young CCA patients (≤ 56 years; p = 0.001), and an absence of lymphatic (p = 0.004) and perineural invasion (p = 0.037), whereas EBP50 was found to be associated with tumor invasion (p = *0*.039), particularly in lymphatic (p < 0.001) and vascular vessels (p < 0.001), as shown in Table 3.2.

Table 3.2 Clinicopathological variables and the expression status of peroxiredoxin 1 (PRX1) and ezrin-radixin-moesin-bindingphosphoprotein 50 (EBP50) in cholangiocarcinoma tissues

Variables	EBP50		*p*	PRX1		*p*
	-ve	+ve		-ve	+ve	
Age(yr)						
≤ 56	69	100	NS	101	68	0.011
> 56	55	75		96	34	
Gender						
Male	79	124	NS	137	66	NS
Female	44	51		59	36	
Histotype group						
Less diff.	104	134	0.039	158	80	NS
Well diff.	15	38		35	18	
Gross type						
Mass forming	60	85	NS	94	51	NS
Periductal infiltrating	22	39		44	17	
Intraductal	5	4		6	3	
Tumor size						
≤ 5 cm	29	45	NS	47	27	NS
> 5 cm	55	74		80	49	

Table 3.2 Clinicopathological variables and the expression status of peroxiredoxin 1 (PRX1) and ezrin-radixin-moesin-bindingphosphoprotein 50 (EBP50) in cholangiocarcinoma tissues (Cont.)

Variables	EBP50		*p*	PRX1		*p*
	-ve	+ve		-ve	+ve	
Tumor invasion						
Absent	79	89	0.019	110	58	NS
Present	35	72		72	35	
Vascular invasion						
Absent	75	59	<0.001	90	44	NS
Present	44	108		100	52	
Lymphatic invasion						
Absent	44	30	<0.001	39	35	0.004
Present	75	135		149	61	
Perineural invasion						
Absent	71	100	NS	103	68	0.037
Present	48	64		85	27	

Note: When the sum of subset numbers does not match patient totals, data were missing or unavailable. Tumor invasion in cholangiocarcinoma (CCA) tissues was diagnosed as positive if the patient fulfilled one of these three criteria: (i) vascular invasion; (ii) lymphatic invasion; or (iii) perineural invasion. NS indicates that the chi-square is not significant using the 0.05 threshold.

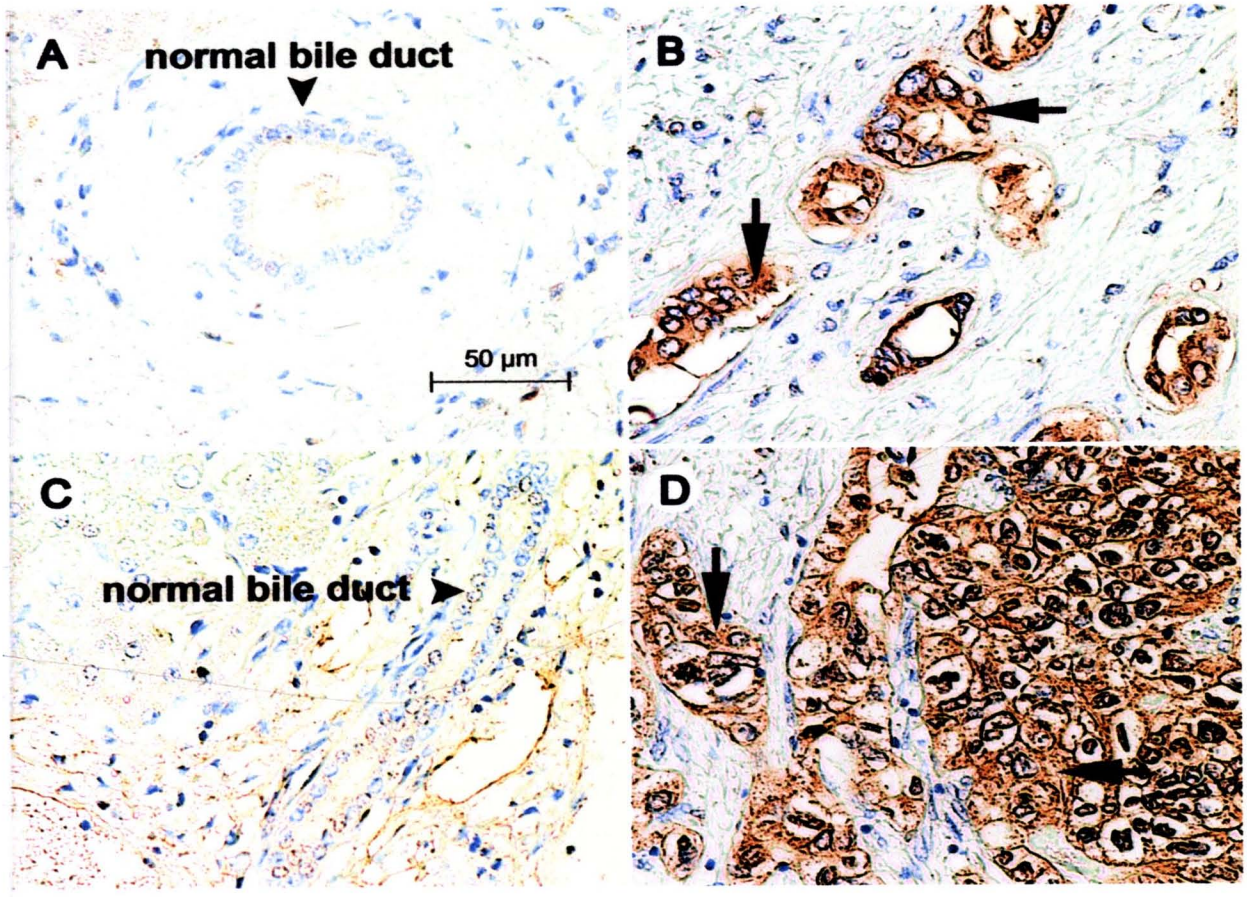

Figure 3.3 Immunohistochemistry of peroxiredoxin 1 (PRX1) and ezrin-radixin-moesin-binding phosphoprotein 50 (EBP50) expression in normal bile duct epithelium and cholangiocarcinoma (CCA). Weak expression of PRX1 (A) and EBP50 (C) was found in human normal cholangiocytes (arrow head), whereas their highly expression were observed mainly in the cytoplasm and on the apical surface of CCA tissues (arrow). Immunoperoxidase staining, original magnification × 200 (A-D).

3.3.4 PRX1 and EBP50 expression and cumulative survival

The median length of survival for patients with high PRX1 expression was 38 weeks (95% CI, 26.10-49.90 weeks) and 29 weeks (95% CI, 23.47-34.53 weeks) for patients with low PRX1 expression. In contrast, the median length of survival for patients with high EBP50 expression was 27.14 weeks (95% CI, 21.68-32.60 weeks) and 38.57 weeks (95% CI, 27.16-49.99 weeks) for patients with low EBP50 expression (Table 3.3). Survival curves for the patients were categorized based on the PRX1 and EBP50 staining categories, and are displayed in Figure 3.4. Diminished survival was seen in the cases with high expression of EBP50 ($p = 0.017$) and low expression of PRX1 ($p = 0.048$).

Table 3.3 Clinical risk factors for overall survival in cholangiocarcinoma patients

Risk factors	Overall survival				
	Univariate analysis (Log-rank)		Multivariate analysis (Cox regression)		
	Median time, wk ± SE (95% CI)	*p*	Relative risk	95%CI	*p*
Histology					
Well differentiated	41.14 ± 6.47 (28.47 - 53.81)	0.029	0.64	0.44-0.92	0.015
Less differentiated	29.00 ± 2.63 (23.85 - 34.15)		1		
Gender					
Male	27.14 ± 1.74 (23.74 - 30.54)	0.025	1.286	0.97-1.71	NS
Female	40.14 ± 4.22 (31.86 - 48.42)		1		
Tumor invasion					
Absent	37.14 ± 4.90 (27.54 -46.74)	0.022	1		
Present	27.42 ± 1.66 (24.17 - 30.67)		1.573	1.18-2.11	0.002
PRX1					
Low expression	29.00 ± 2.82 (23.47 - 34.53)	0.048	1.511	1.14-2.01	0.004
High expression	38.00 ± 6.07 (26.10 - 49.90)		1		
EBP50					
Low expression	38.57 ± 5.82 (27.16 - 49.99)	0.017	0.734	0.56-0.96	0.025
High expression	27.14 ± 2.79 (21.68 - 32.60)		1		

Note: CI, confident interval; NS, not significant.

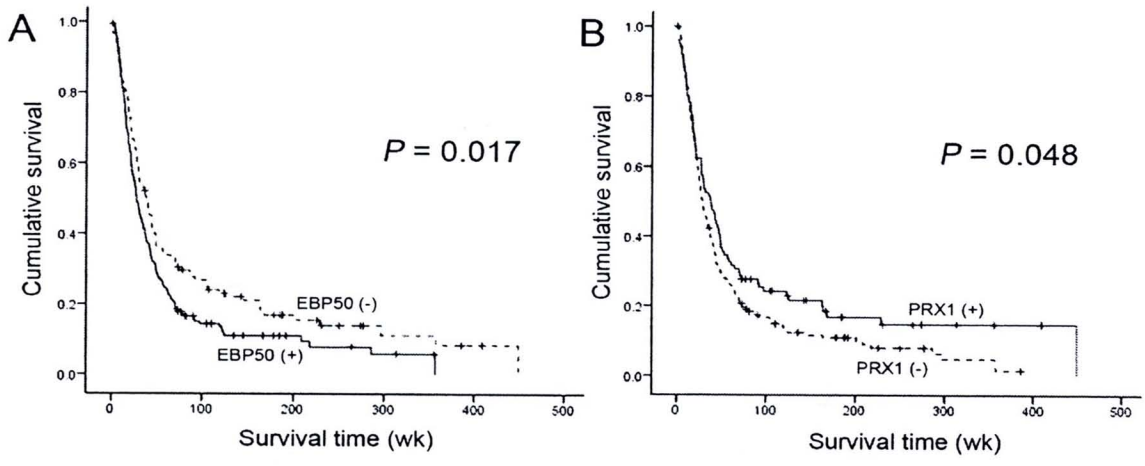

Figure 3.4 Kaplan-Meier cumulative survival curves for overall survival of *Opisthorchis viverrini*-associated cholangiocarcinoma (CCA) patients according to the expression status of ezrin-radixin-moesin-binding phosphoprotein 50 (EBP50) (A) and peroxiredoxin 1 (PRX1) (B) in primary tumors.

3.4 Discussion

Identification of protein profiles is important for understanding the mechanisms of cholangiocarcinogenesis and could facilitate the development of new tools for the diagnosis, treatment and prevention of CCA. In this study, we applied a proteomics-based approach to identify differentially expressed tumor proteins in CCA cell lines. Up-regulation of peroxiredoxin 1 (PRX1), ezrin and moesin in moderately differentiated (M156) but not in poorly differentiated (K100) CCA cell lines might imply a potential association with the improved prognosis of CCA patients. However, a drawback to this methods is that cells line are not representative of the tissue of origin as they they have been maintained and propagated *in vitro* for extended time periods (Hay et al., 1988). Furthermore, each cell line was established from a few cells of a single patient biopsy; hence, these cells lines may not accurately represent the overall tumor characteristics (Hay et al., 1988). Accordingly, validation of comparative proteomic results from the cell lines in the patient biopsies is an important step in developing prognostic markers for CCA. Therefore, PRX1 and ezrin-radixin-moesin-binding phosphoprotein 50 (EBP50), which is a binding partner

of ezrin and moesin, were selected for further verification using IHC analysis on TMA of CCA tissues, as their expression levels have been shown to correlate with carcinogenesis in other cancers (Kim et al., 2007; Song et al., 2007; Georgescu et al., 2008; Chhipa et al., 2009).

Peroxiredoxins are found in mammals, yeast, and bacteria, and are characterized as thiol-specific antioxidant proteins. They are further classified as possessing either one (1-Cys) or two (2-Cys) conserved cysteine residues (Rhee et al., 2001). The catalytic mechanism of the 2-Cys peroxiredoxins, particularly PRX1, is specific among the peroxide-detoxifying enzymes (Kim et al., 2006). The function of PRX1 in particular has been implicated in regulating cell proliferation, differentiation, and apoptosis (Cha et al., 2009).

Over-expressions of PRX1 have been observed in several human cancers, i.e. lung, breast, esophagus, oral, and thyroid (Yanagawa et al., 1999; Yanagawa et al., 2000; Noh et al., 2001). The up-regulation of PRX1 has been linked to tumor suppression in oral squamous cell cancer as reported by Yanagawa et al. (Yanagawa et al., 2000) that low levels of PRX1 expression associated with larger tumor masses, lymph node metastases, and poorly differentiated cancers. However, the connection between PRX1 and bile duct cancer has not yet been clearly defined. Our IHC analysis showed an association between the over-expression of PRX1 in human *O. viverrini*-associated CCA and a decrease in tumor invasion in lymphatic and vascular vessels. The expression of PRX family members is induced by oxidative stress (Chang et al., 2001), Pinlaor et al. (Pinlaor et al., 2004a; Pinlaor et al., 2004b) reported a number of evidences regarding a model of inflammation-mediated cholangiocarcinogenesis via NO-mediated oxidative and nitrative DNA damage in hamsters infected with *O. viverrini*.

Furthermore, we have identified ezrin and moesin, members of ezrin-radixin-moesin (ERM) family in which have been reported as a ligand for EBP50 or Na+/H+ exchanger regulatory factor (Waisman, 1995; Reczek et al., 1997). EBP50 is an adapter molecule containing two tandem post-synaptic density-95/Disk-large/ZO-1 homologous (PDZ) domains that can bind integral membrane proteins and the N-terminal ERM association domain (N-ERMAD) of ERM proteins (Song et al.,

2007) promoting the assembly of membrane-bound macromolecular complexes involved in signal transduction (Maudsley et al., 2000).

Although EBP50 was first hypothesized as a mitogenic factor, it was later shown to act as an oncogene (Maudsley et al., 2000; Shibata et al., 2003; Lazar et al., 2004; Cardone et al., 2007) or as a tumor suppressor gene (Lazar et al., 2004; Takahashi et al., 2006; Kreimann et al., 2007; Wang et al., 2008) regarding to its distribution. Recent studies report that EBP50 may act as a tumor suppressor by interacting with β–catenin and stabilizing adherent junctions or by forming a triple complex with PTEN and platelet-derived growth factor receptor at the cell membrane of epithelial cells, and thereby exerting an inhibitory action on PI3K signaling (Takahashi et al., 2006; Pan et al., 2008). However, over expression and intracellular delocalization of EBP50 can break up complexes with PTEN or β-catenin and also scaffold complexes in the cytoplasm and/or nucleus, thus separating signaling molecules away from the plasma membrane exerting tumor progression (Georgescu, 2008). In addition, EBP50 has been reported to be over expressed and redistributed to the cytoplasm and/or nucleus of proliferative cells in hepatocellular carcinoma (Shibata et al., 2003) and in estrogen stimulated tissues such as in endometrium and breast cancers (Stemmer-Rachamimov et al., 2001; Cardone et al., 2007; Song et al., 2007). Consistent with this possibility, we herein found that over-expression of EBP50 was clearly visualized in both the cytoplasm and membrane of CCA tissues and its expression was also associated with tumor invasion in lymphatic and vascular vessels.

A Cox-regression model (as shown in Table 3.3) showed that PRX1, EBP50, histology type and tumor invasion were associated with a longer survival time after surgery. More specifically (Table 3), patients with low expression of EBP50 and high expression of PRX1 had longer survival times after surgery compared with patients with high expression of EBP50 and low expression of PRX1, respectively. Regarding tumor invasion and metastasis, it has been reported that the survival time after surgery for the group with the presence of tumor invasion and metastasis was shorter than the group with absence of tumor invasion and metastasis in CCA (Uttaravichien et al., 1999). In addition, it was also demonstrated that the patients with well differentiated histophathological type of CCA had longer survival times after surgery compared to the less differentiated type (Nathan et al., 2007).